






Article

Co₃O₄-rGO—Synthesis, Characterization, and Evaluation of Photocatalytic Activities

Muhammad Saeed ^{1,*}, Firas H. Albadran ², Ameer Fawad Zahoor ¹, Asif Nisar ¹, Aamal A. Al-Mutairi ³, Sami A. Al-Hussain ³, Ali Irfan ¹ and Magdi E. A. Zaki ^{3,*}

- ¹ Department of Chemistry, Government College University, Faisalabad 38000, Pakistan; fawad.zahoor@gcuf.edu.pk (A.F.Z.); asifnisar52@yahoo.com (A.N.); raialiirfan@gmail.com (A.I.)
- ² Department of Chemical and Petroleum Refining, Engineering College of Oil and Gas Engineering, Basrah University for Oil and Gas, Basrah 61004, Iraq; albadran.f@buog.edu.iq
- ³ Department of Chemistry, College of Science, Imam Mohammad Ibn Saud Islamic University (IMSIU), Riyadh 11623, Saudi Arabia; aamutairi@imamu.edu.sa (A.A.A.-M.); sahussain@imamu.edu.sa (S.A.A.-H.)
- * Correspondence: msaeed@gcuf.edu.pk (M.S.); mezaki@imamu.edu.sa (M.E.A.Z.)

Abstract: Water contamination with synthetic dyes is an escalating problem worldwide. Herein, Co₃O₄-decorated reduced graphene oxide (Co₃O₄-rGO) is reported as an effective heterogeneous photocatalyst for the decomposition of organic dyes. The synthesis of Co₃O₄-rGO was confirmed via spectroscopic techniques including XRD, XPS, TEM, and FTIR. After characterization, the prepared Co₃O₄-rGO composite was tested as a photocatalyst for the degradation of methylene blue and methyl orange. The photocatalytic efficiency of Co₃O₄-rGO was >95% after 60 min, corresponding to 200 mg/L as the initial concentration of each dye. The photodegradation of MB and MO was confirmed by BOD and COD measurements. Experimental parameters like the re-usability of Co₃O₄-rGO, the effect of catalyst dosage, and the effect of dye concentration on photocatalytic activity were also investigated. The photocatalytic activity of Co₃O₄-rGO for the degradation of MB was 2.13 and 3.43 times higher than that of Co₃O₄ and rGO, respectively. Similarly, the photocatalytic activity of Co₃O₄-rGO for the degradation of MO was 2.36 and 3.56 times higher than that of Co₃O₄ and rGO, respectively. Hence, Co₃O₄-rGO was found to be an efficient and reusable photocatalyst for the decomposition of selected dyes in the aqueous medium.

Keywords: methylene blue; methyl orange; Co₃O₄-rGO; photodegradation



Citation: Saeed, M.; Albadran, F.H.; Zahoor, A.F.; Nisar, A.; Al-Mutairi, A.A.; Al-Hussain, S.A.; Irfan, A.; Zaki, M.E.A. Co₃O₄-rGO—Synthesis, Characterization, and Evaluation of Photocatalytic Activities. *Catalysts* **2024**, *14*, 96. <https://doi.org/10.3390/catal14020096>

Academic Editor: Bo Weng

Received: 21 December 2023

Revised: 9 January 2024

Accepted: 15 January 2024

Published: 24 January 2024



Copyright: © 2024 by the authors. Licensee MDPI, Basel, Switzerland. This article is an open access article distributed under the terms and conditions of the Creative Commons Attribution (CC BY) license (<https://creativecommons.org/licenses/by/4.0/>).

1. Introduction

Recently, catalysis in general and photocatalysis employing semiconductors as heterogeneous catalysts and sunlight as a source of energy in particular have received considerable attention due to a wide range of applications [1–5]. The photocatalytic reactions are comprised a series of oxidation and reduction reactions mediated by positive holes and electrons formed in the valence band and conduction band of semiconductor catalysts under irradiation with ultraviolet or visible light [6–9]. Among the photocatalytic redox reactions, the UV–visible light-assisted decomposition reactions of organic pollutants like dyes are the most reported. The overexploitation of limited resources and rapid industrial development due to human activities have increased water pollution globally [10]. Although many traditional methods like membrane filtration, adsorption, biological and chemical coagulation, and precipitation are used for the abatement of aqueous pollution, these techniques are not successful in the complete removal of pollutants from the environment [11–14]. These methods transform the pollutants from one phase to another. Therefore, the abatement of pollution due to organic dyes via photocatalytic reactions has received much attention from researchers worldwide.

ZnO and TiO₂ have been mostly used as single-component semiconductor photocatalysts for the photodegradation of dyes and other organic pollutants [15,16]. However,

the practical applications of these semiconductor metal oxides are limited due to certain characteristics. The characteristics that limit their practical applications include insufficient absorption of visible light, poor photostability, and lower separation efficiency of photo-induced charges. Thus, researchers have focused on the development of multi-component visible light-active photocatalysts with enhanced charge separation efficiency [17–23]. The literature has shown that dopants, co-catalysts, and carbonaceous materials have been widely used for the development of multi-component photocatalysts with enhanced photocatalytic activity [24,25]. Hence, the immobilization of cobalt oxide on reduced graphene is reported in this study for the development of an efficient Co_3O_4 -rGO photocatalyst. Cobalt oxide is a suitable semiconductor for the development of an effective photocatalyst due to its narrow band gap (~2.7 eV), exciting magnetic properties, fascinating catalytic properties, high chemical and thermal stability, and ease of preparation. The photocatalytic activities of Co_3O_4 can be enhanced by supporting them on the surface of graphene oxide. The synergistic effects of graphene oxide suppress the recombination of photoinduced charges, resulting in the enhancement of photocatalytic performance. It has been reported by many researchers that linking semiconductor metal oxides to graphene oxide suppresses the recombination of charge carriers formed by the absorption of photons and subsequently results in a significant enhancement in the photocatalytic performance. The graphene oxide in the metal oxide-graphene oxide composite acts as an electron mediator. As a result, the photoinduced charge carriers (h^+ / e^-) are effectively separated. The effective separation of these photon-induced charge carriers causes an enhancement in the photocatalytic performance of the composite [26,27]. Therefore, we immobilized the Co_3O_4 particles on the surface of rGO to obtain an efficient, visible light-driven photocatalyst for the decomposition of selected synthetic dyes. The contribution of synthetic dyes to water pollution is very significant. The wastewater contaminated with synthetic dyes originates from different industries like the paint, tannery, paper, printing, and textile industries. Wastewater contaminated with synthetic dyes is very toxic for life. Methylene blue and methyl orange are typical cationic synthetic dyes used in various industries [28,29]. In this study, we report the photodegradation of methylene blue and methyl orange in the presence of Co_3O_4 -rGO under the irradiation of visible light.

2. Results and Discussion

2.1. Characterization of Co_3O_4 -rGO

The formation of Co_3O_4 -rGO was confirmed via XRD as the initial characterization technique. XRD analyses of rGO and Co_3O_4 were also carried out for comparison. Figure 1 shows the XRD patterns of the samples. The XRD pattern of rGO comprised peaks at 2θ , 24.2° , and 42.8° , which are related to the (002) and (100) planes of rGO. Similarly, the XRD pattern of Co_3O_4 comprised diffraction peaks at 2θ , 36.34° , 38.56° , 44.8° , 59.35° , 65.23° , 77.34° , and 78.4° , which correspond to the (2 2 0), (3 1 1), (2 2 2), (4 0 0), (5 1 1), (6 2 0), (5 1 1), (5 3 3), and (6 2 2) planes of Co_3O_4 (JCPDS Card No. 42-1467). The XRD pattern of Co_3O_4 -rGO matches well with the XRD patterns of rGO and Co_3O_4 , which confirms the successful formation of the Co_3O_4 -rGO composite [30–33].

The average crystallite size of Co_3O_4 -rGO was calculated at 43.5 nm using the Debye–Scherrer equation (Equation (1)). The hkl planes and corresponding angles of diffraction (2θ) in XRD patterns were used for the calculation of lattice parameters of the cubic structure of the unit cell using Equation (2) via the non-linear method of analysis. The “Solver” add-in software of MS Excel was used for this purpose. The lattice parameters for the cubic structure were calculated as $a = b = c = 11.98 \text{ \AA}$.

$$d = \frac{0.98 \times 1.54}{\beta \cos \theta} \quad (1)$$

$$\frac{1}{d_{hkl}^2} = \frac{h^2 + k^2 + l^2}{a^2} \quad (2)$$

The formation of Co_3O_4 -rGO was further confirmed using XPS analysis. Figure 2 shows the XPS spectra of Co, O, and C, which confirms the existence of Co, O, and C in the prepared sample. Figure 2a displays the XPS spectrum of Co(2p), in which two peaks can be observed. The first peak at 780.3 eV is ascribed to $\text{Co}(2p_{3/2})$, while the second peak at 795.8 eV is ascribed to $\text{Co}(2p_{1/2})$. These peaks confirm the +3 oxidation state of Co in the composite [30]. The high-resolution deconvoluted XPS spectrum for the O 1s region given in Figure 2b showed three peaks at binding energies of 529.7 (OI), 531.0 (OII), and 532.0 (OIII) eV, which are assigned to typical metal–oxygen bonds on the Co_3O_4 surface with low oxygen coordination. The latter two signals are typical peaks of O-Co linkages. Figure 2c depicts the deconvoluted C1s XPS spectrum, indicating three signals at 284.0, 288.3, and 294.0 eV. The existence of three signals suggests three different electronic environments. The peak observed at 288.3 eV is a typical peak for graphene oxide [34–36].

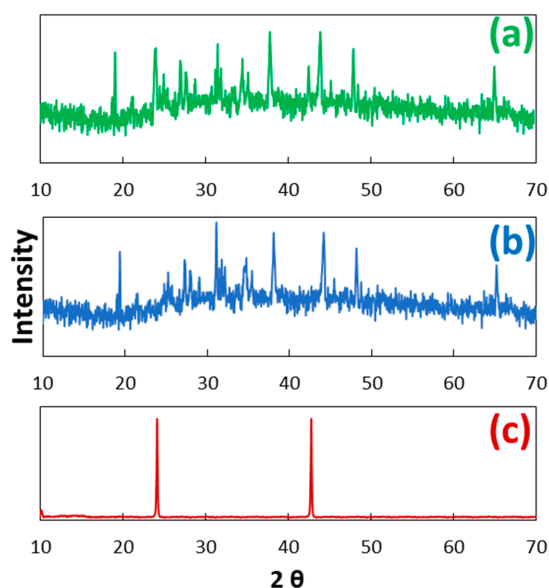


Figure 1. XRD, (a) Co_3O_4 -rGO, (b) Co_3O_4 , and (c) rGO.

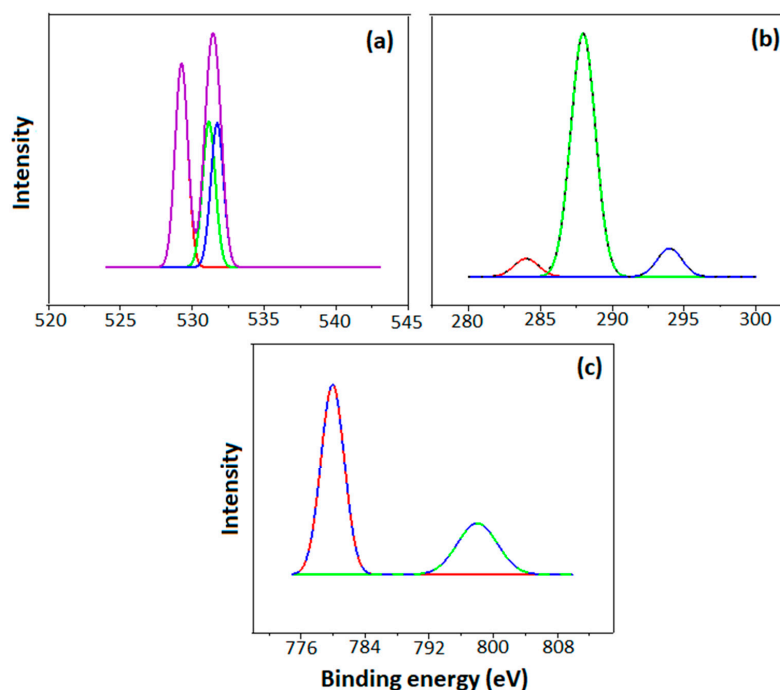


Figure 2. XPS spectra of (a), O (b) C, and (c) Co.

The morphology of Co_3O_4 -rGO was investigated by transmission electron microscopy. The transmission electron micrographs of the sample are given in Figure 3. It can be observed that the rGO in the Co_3O_4 -rGO composite is a thin, flat flake with a crumpled morphology. The existence of crumpled sheets and thin multilayers is associated with the exfoliation process in sonification and reduction. A slight aggregation of Co_3O_4 nanoparticles can be observed, which confirms that Co_3O_4 nanoparticles have been successfully anchored to the surface of rGO. The attachment of Co_3O_4 to the rGO suppresses the aggregation of Co_3O_4 particles; hence, the rGO is a suitable substrate for the improvement of the dispersion, stability, and photocatalytic performance of Co_3O_4 -rGO [37,38].

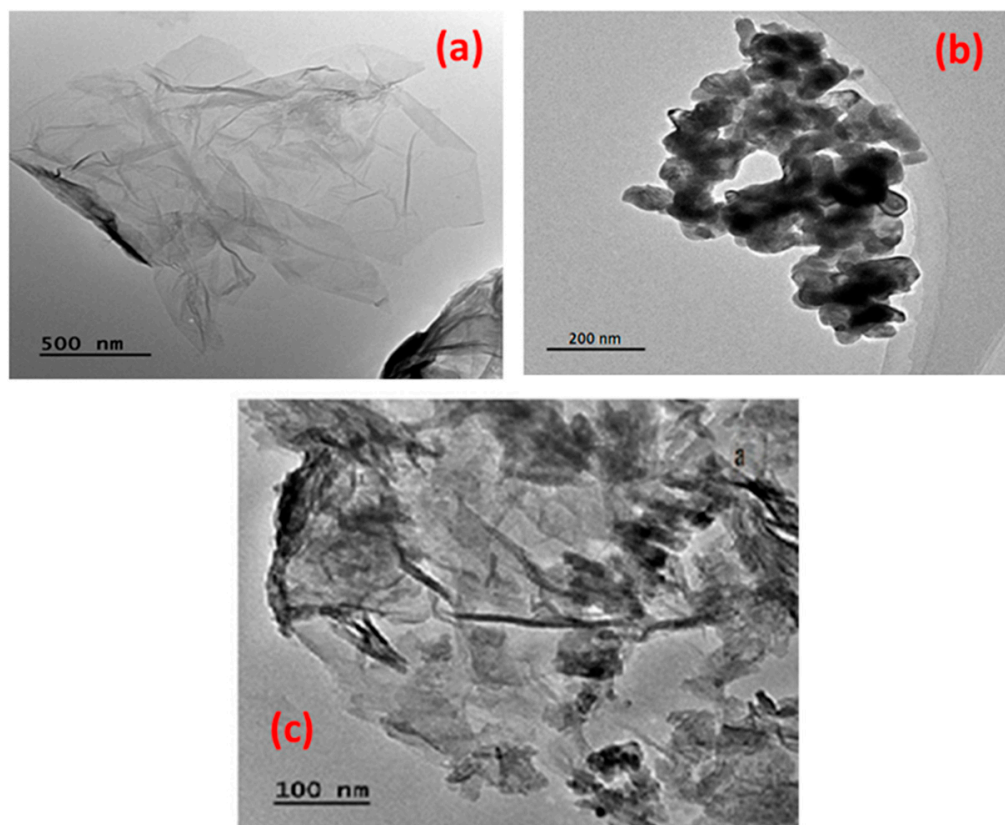


Figure 3. TEM analysis; (a) rGO, (b) Co_3O_4 , and (c) Co_3O_4 -rGO.

The FTIR spectra of Co_3O_4 , rGO, and Co_3O_4 -rGO are given in Figure 4. The observed peak at 3404 cm^{-1} is due to the stretching vibration of O-H, and the peak at 1740 cm^{-1} showed the stretching vibration of the (C=O) carboxyl group. A broad band in the range of $1475\text{--}1543\text{ cm}^{-1}$ is indexed to C-O as a vibration corresponding to rGO and also surface-decorated Co_3O_4 via the C-O bond. The absorption band at 1023 cm^{-1} is due to C-O stretching vibration, while at 1623 cm^{-1} , it corresponds to the C=C bond. The O-H band was moved to 3424 cm^{-1} for the Co_3O_4 -rGO composite, and the band of the skeletal vibration of C=C was shifted to 1627 cm^{-1} [25,39]. The band appearing at 565 and 661 cm^{-1} in the FTIR spectrum of Co_3O_4 has been indexed to the Co-O vibration mode. These peaks have been shifted to 600 and 678 cm^{-1} in the presence of rGO [30].

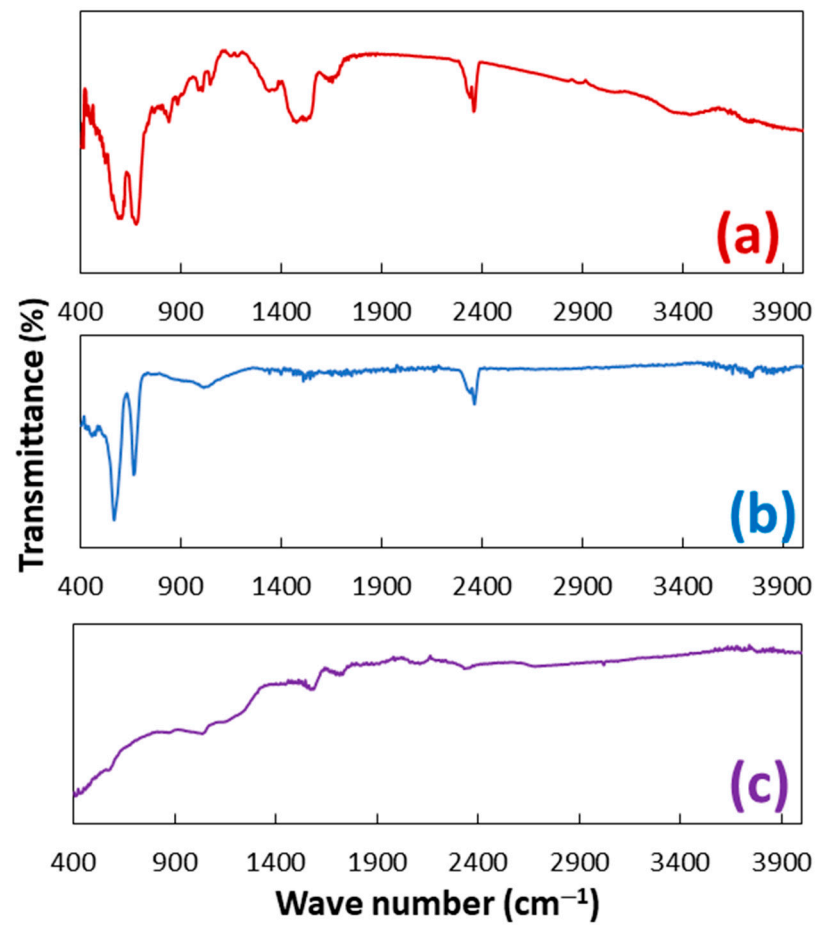


Figure 4. FTIR spectrum of (a) Co₃O₄-rGO, (b) Co₃O₄, and (c) rGO.

The band gap energy of Co₃O₄-rGO was calculated using the UV–visible DR spectrum as given in Figure 5. Using 470 nm as the absorption edge and the equation given in Figure 5, the band gap energy of Co₃O₄-rGO was calculated at 2.63 eV, which is comparable to reported data [7].

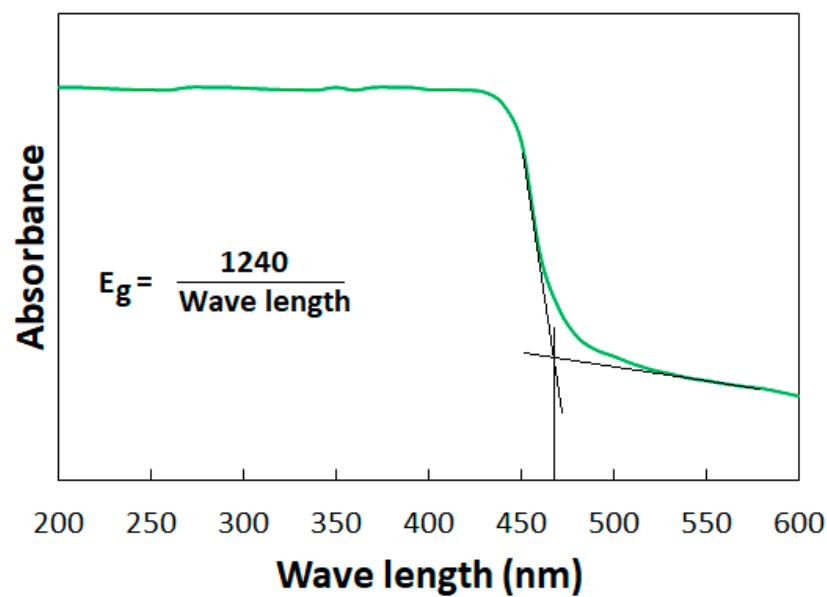


Figure 5. UV–DR spectrum of Co₃O₄-rGO.

2.2. Photocatalytic Efficiency of Co_3O_4 -rGO

The photocatalytic efficiency of the as-prepared Co_3O_4 -rGO photocatalyst was assessed through the investigation of the photodegradation of methylene blue (MB) and methyl orange (MO) dyes. The photocatalytic experiments were carried out using a dye solution of 50 mL with an optimum value of 0.1 g of the photocatalyst under irradiation with UV–visible light. Before the evaluation of photocatalytic activity, two blank experiments were performed.

In the first blank experiment, 50 mL of 200 mg/L of MB or MO solution was taken in a Pyrex glass beaker. A sample of 0.5 mL was taken from the beaker, and its absorbance was noted after dilution. The dye solution was then stirred under UV–visible light for 1 h to detect any degradation due to photolysis. After stirring for one hour, a sample was taken and analyzed. It was found that there was no change in the concentration of the dye due to stirring under irradiation. Hence, there was no degradation of either dye due to photolysis.

In the second blank experiment, 0.1 g of the catalyst (rGO, Co_3O_4 , or Co_3O_4 -rGO) was added to the MB or MO dye solution (50 mL, 200 mg/L), and the reaction mixture was stirred for half an hour under dark conditions. This blank experiment was performed for the estimation of the removal of dye due to adsorption. After half an hour, a sample was taken, and its absorbance was measured. The analyses of the data showed that there was about 14, 20, and 32% removal of each dye due to adsorption on rGO, Co_3O_4 , and Co_3O_4 -rGO, respectively. The elimination of MB and MO due to sorption is shown in Figure 6a.

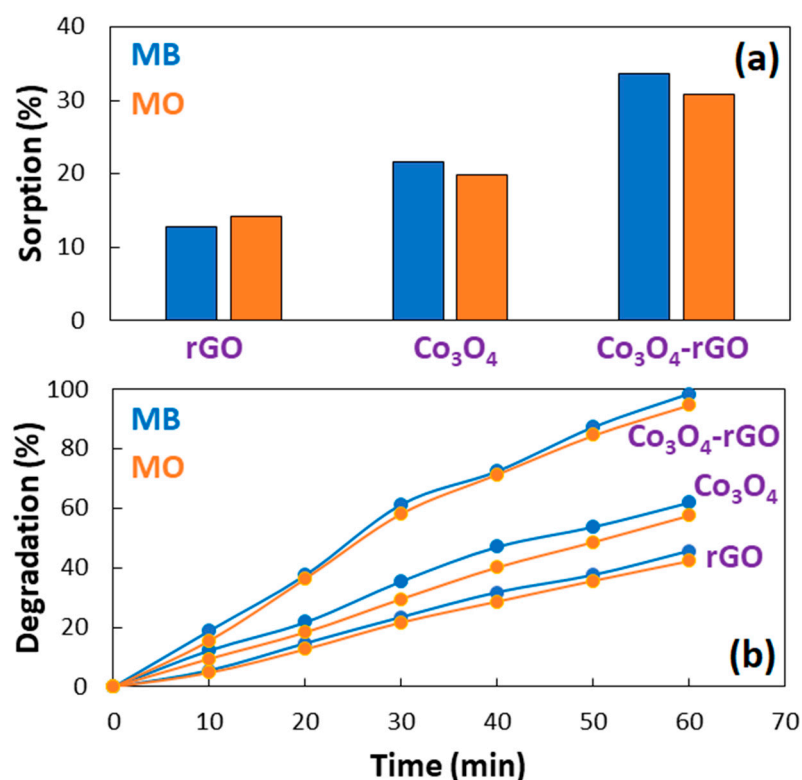


Figure 6. Removal of MB and MO dyes over Co_3O_4 , rGO, and Co_3O_4 -rGO (a) via sorption and (b) via photocatalysis.

After two blank experiments, the reaction mixture was stirred under UV–visible irradiation for the evaluation of the photocatalytic activity of each sample. The absorbance measured after stirring for 30 min in the dark was considered the initial absorbance for the evaluation of the photocatalytic activity. The photodegradation of MB and MO over rGO, Co_3O_4 , and Co_3O_4 -rGO is given in Figure 6b. About 98, 62, and 45% photodegradation of methylene blue was observed in 60 min of reaction using Co_3O_4 -rGO, Co_3O_4 , and rGO

as photocatalysts, respectively. Similarly, the photodegradation of methyl orange was 92, 57, and 42% over Co_3O_4 -rGO, Co_3O_4 , and rGO as photocatalysts, respectively. The photodegradation data demonstrated that the incorporation of Co_3O_4 in reduced graphene oxide sheets increased the photocatalytic ability of the composite toward the degradation of MB and MO dyes.

The photocatalytic degradation of the selected dyes was confirmed via COD and BOD measurements as well. About 80% and 68% reductions in COD and BOD were detected in the 50 mL (200 mg/L) solution of MB/MO after treatment with Co_3O_4 -rGO for 60 min. The decrease in COD and BOD of the dye solutions indicates that Co_3O_4 -rGO can be employed as an efficient catalyst for the photodegradation of the dyes.

The re-usability of Co_3O_4 -rGO in the photodegradation of MB and MO was also investigated. For this purpose, the spent Co_3O_4 -rGO was washed with ethanol and distilled, followed by drying at 80 °C overnight. The regenerated Co_3O_4 -rGO was employed as a catalyst in separate photodegradation experiments of MB and MO for 30 min. The spent Co_3O_4 -rGO was recycled three times. The results indicated that there was no significant loss in the photocatalytic activity of Co_3O_4 -rGO. The obtained results confirmed that Co_3O_4 -rGO can be re-used in the photodegradation of MB and MO.

2.3. Optimization of Catalyst Dose

The unnecessary use of a catalyst can be avoided by employing the optimum dosage of the catalyst. The optimization of catalyst dosage was accomplished by performing photodegradation experiments using a 50 mL (200 mg/L) solution of MB or MO with different catalyst dosages in the range of 0.05–0.2 g Co_3O_4 -rGO under similar experimental conditions. The obtained results are given in Figure 7. The data given in Figure 7 show that photocatalytic activity initially increased with catalyst dosage and then decreased. Initially, the photocatalytic activity increased with catalyst dosage because the number of active sites of the catalyst increased with catalyst dosage. However, higher catalyst dosages caused a decrease in photocatalytic activity. This is because photons cannot penetrate effectively through the scattering of photons and the turbidity of the reaction mixture. Hence, 0.1 g was selected as the optimum catalyst dose in this study [40,41].

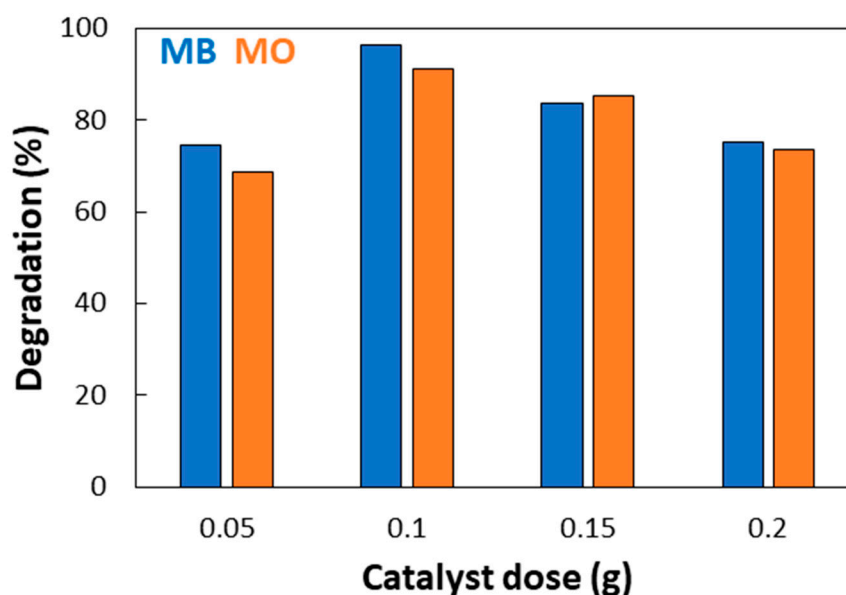


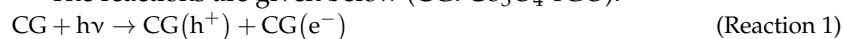
Figure 7. Optimization of catalytic dosage of Co_3O_4 -rGO in photodegradation of MB and MO.

2.4. Mechanism and Kinetics of Photodegradation

Figure 8 explains the mechanism of photodegradation. Photodegradation is based on the excitation of both the dye and the photocatalyst. The irradiation of the dye solution

results in the excitation of the dye molecules. The excited electrons then flow to the conduction band of Co_3O_4 via rGO sheets. Similarly, the excitation of Co_3O_4 results in the formation of positive holes and electrons in the conduction band and valence band, respectively. The intermediate work function of rGO (-4.42 eV) between the conduction band (-3.40 eV) and valence band (-6.65 eV) of Co_3O_4 causes a flow of electrons to the rGO. Hence, the positive holes and electrons are separated, resulting in a decrease in the rate of their recombination. These separated positive holes and electrons then undergo a series of reactions and produce OH radicals [42–45].

The reactions are given below (CG: Co_3O_4 -rGO).



As indicated in the above-mentioned reactions, positive holes, electrons, and hydroxyl radicals are the main species responsible for the photodegradation of dyes; therefore, the formation of these charge carriers was confirmed via scavenging experiments. For this purpose, separate photodegradation experiments were performed in the presence of EDTA, BQ, and t-BuOH. These species were added to a reaction mixture to arrest positive holes, superoxide anion radicals, and hydroxyl radicals, respectively. The photocatalytic activity of Co_3O_4 -rGO towards the degradation of MB decreased from 98% to 67, 61, and 49% in the presence of EDTA, BQ, and t-BuOH, respectively. The decline in photocatalytic performance in the presence of EDTA is due to the non-availability of positive holes for the photodegradation reaction. Similarly, the decrease in photocatalytic performance in the presence of BQ and t-BuOH is due to the non-availability of superoxide anion and hydroxyl radicals, respectively [46,47].

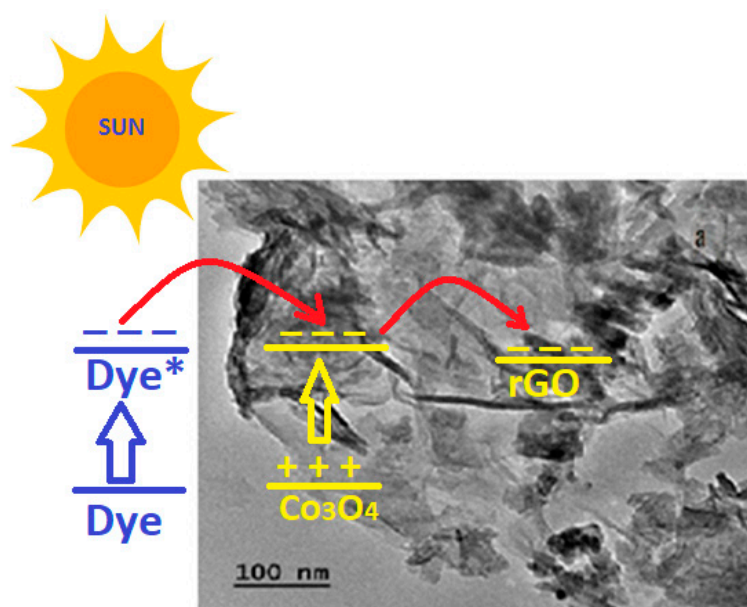


Figure 8. Mechanism of photodegradation of dyes in the presence of Co_3O_4 -rGO. * is the excitation of the dye molecules.

Based on reaction 7, the rate of reaction can be written as

$$\text{Rate} = -\frac{d[\text{Dy}]}{dt} = k_r[\text{OH}][\text{Dy}]^n \quad (3)$$

For the same catalyst dosage and continuous irradiation of the reaction mixture, the rate of formation of OH radicals or the concentration of OH radicals will remain the same; hence, the rate expression is modified as follows (where k is the apparent rate constant).

$$\text{Rate} = -\frac{d[Dy]}{dt} = k[Dy]^n \quad (4)$$

Considering the first order reaction ($n = 1$), the rate expression is written as

$$\ln \frac{[Dy]_0}{[Dy]_t} = k t \quad (5)$$

$$[Dy]_t = [Dy]_0 e^{-k t} \quad (6)$$

The photodegradation data of MB and MO, as given in Figure 6b, were analyzed using a non-linear method of analysis according to the kinetics Equation (6). For non-linear analyses, the Excel “Solver” add-in optimization software was used. The non-linear analyses of the photodegradation data are given in Figure 9. The rate constants and correlation coefficients are given in Table 1. The rate constants given in Table 1 show that the photocatalytic activity of Co_3O_4 -rGO for degradation of MB is 2.13 and 3.43 times higher than that of Co_3O_4 and rGO, respectively. Similarly, the photocatalytic activity of Co_3O_4 -rGO for the degradation of MO is 2.36 and 3.56 times higher than that of Co_3O_4 and rGO, respectively.

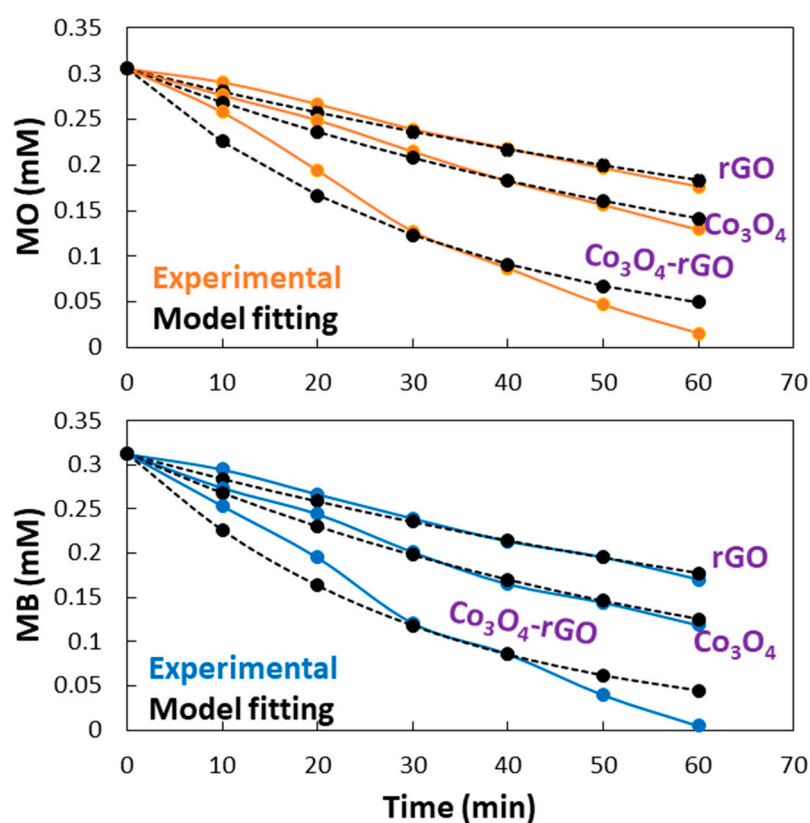


Figure 9. Kinetics analyses of the photodegradation data.

Table 1. Rate constants determined using non-linear analyses.

Photocatalyst	MB		MO	
	k	R ²	k	R ²
rGO	0.0094	0.995	0.0085	0.995
Co ₃ O ₄	0.0152	0.992	0.0128	0.994
Co ₃ O ₄ -rGO	0.0323	0.983	0.0303	0.985

2.5. Effect of Dye Concentration

In wastewater treatment, the concentration of the dye is a very vital parameter because the concentration significantly affects the efficiency of the method used for its removal. To study the effect of dye concentration, photodegradation experiments involving methylene blue and methyl orange were carried out with various dye concentrations such as 100, 200, and 300 mg/L in the presence of a Co₃O₄-rGO photocatalyst. The dependence of photocatalytic efficiency on the concentration of dyes was examined for the photo-degradation of MB and MO separately using 0.1 g of the Co₃O₄-rGO photocatalyst. The results obtained from the degradation of MB and MO are shown in Figure 10. The rate constants determined using kinetics analyses are given in Table 2. The degradation data given in Figure 10 and the rate constants given in Table 2 show that the photocatalytic efficiency of the catalyst decreased with an increase in dye concentration. The decrease in photocatalytic activity with an increase in the concentration of the dyes is due to the following reasons [48–50]:

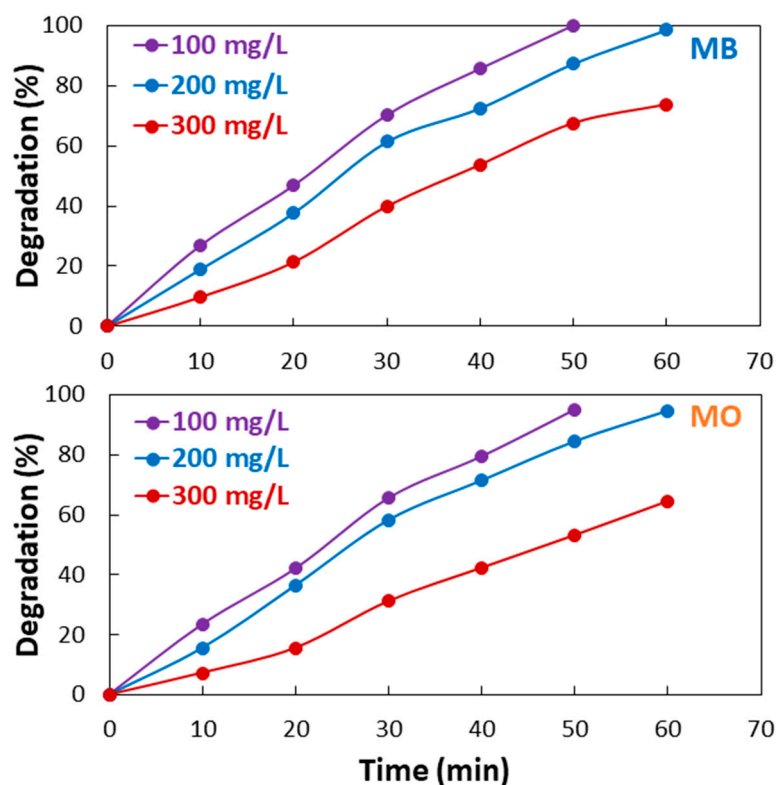
**Figure 10.** Effect of dye concentration on photocatalytic efficiency of Co₃O₄-rGO photocatalyst.

Table 2. Effect of dye concentration on the rate constant of Co_3O_4 -rGO-catalyzed photodegradation of dyes.

Concentration (mg/L)	MB		MO	
	k	R ²	k	R ²
100	0.0432	0.991	0.0363	0.991
200	0.0323	0.983	0.0303	0.985
300	0.0206	0.987	0.0151	0.988

(1) As dyes impart an intense color to the solution, the penetration of photons is hindered due to the intense color.

(2) The ratio of dye molecules to OH radicals increases with an increase in the concentration of dye.

Finally, the photocatalytic activity of Co_3O_4 -rGO reported in this study was compared with the photocatalytic activities of various graphene-based photocatalysts used for the degradation of various dyes reported in the previous literature. Table 3 shows a comparison of the photocatalytic activities of various graphene-based catalysts for different dyes. It can be concluded that the graphene-based catalyst reported in this study is effective for the photodegradation of methylene blue and methyl orange dyes.

Table 3. Graphene-based photocatalysts reported in the literature for degradation of various dyes.

No	Graphene-Catalyst	Dye	Activity
1	Ag [51]	MB RhB	Almost complete degradation in 70 min using 10 mg/L of dye solution
2	BiOBr [52]	RhB	Almost complete degradation in 5 h using 20 mg/L dye solution
3	MoS ₂ [53]	MB	A 99% degradation in 60 min using 10 mg/L dye solution
4	CeO ₂ [54]	RhB	An 85% degradation in 2 h using 10 mg/L dye solution
5	ZnO [55]	MO	A 92% degradation in 3 h using 5 mM dye solution
6	Cu ₂ O [56]	MO	A 70% degradation in 5 h using 5 mg/L dye solution
7	TiO ₂ [57]	MO	A 90% degradation in 5 h using 10 mg/L dye solution
8	CoFe ₂ O ₄ [58]	MO	A 78% degradation in 30 min using 10 mg/L dye solution
9	Au [59]	MB (10 mg/L)	Almost complete degradation in 10 min using 10 mg/L dye solution
10	Co ₃ O ₄ (this work)	MB MO	Complete degradation in 60 min using 100 mg/L dye solution

3. Experimental Process

3.1. Reagents

The chemicals used in this study include sodium nitrate (Merck, Rahway, NJ, USA), graphite powder (Merck), sulfuric acid (Scharlau, Hamburg, Germany), potassium permanganate (Merck), hydrogen peroxide (30%, commercial grade), cobalt nitrate (Merck), sodium borohydride (Merck), sodium hydroxide (Merck), methylene blue (Sigma-Adrich, Saint Louis, MO, USA), and methyl orange (Sigma-Adrich).

3.2. Synthesis of Co_3O_4 -rGO

In the first step, graphene oxide (GO) was synthesized. For this purpose, 2 g of sodium nitrate and 4 g of graphite were added to 100 mL of concentrated sulfuric acid. After stirring for 30 min in an ice-cold bath, 14 g of potassium permanganate was slowly added while stirring, keeping the temperature below 20 °C. After 4 h of stirring, a thick paste was formed. Then, 200 mL of distilled water was added while stirring. As a result, the temperature rose to 98 °C, and a yellowish suspension was formed. The reaction was stopped through the addition of hydrogen peroxide, and the obtained product, designated as graphene oxide (GO), was washed and dried.

In the second step, Co_3O_4 -rGO was synthesized. For this purpose, a 60 mL solution containing 0.043 g of cobalt nitrate was added to a 60 mL suspension containing 0.08 g of previously prepared graphene oxide, followed by ultrasonication. Then, 0.28 g of sodium borohydride was added to the above mixture. A total of 0.1 M sodium hydroxide solution was added slowly until pH reached 11. After 60 min, black precipitates were obtained via centrifugation and washed multiple times with triply distilled water and ethanol. The precipitates were desiccated in a vacuum oven at 98 °C.

Reduced graphene oxide (rGO) was also synthesized for comparison. For this purpose, 70 mg of sodium borohydride was added to a suspension of already-prepared graphene oxide. After sonication and stirring, the rGO was collected, washed, and dried.

3.3. Characterization of Co_3O_4 -rGO

The successful synthesis of Co_3O_4 -rGO was verified using various characterization techniques, such as XRD, XPS, TEM, and FTIR. The XRD analyses were carried out with a Bruker X-ray diffractometer (Bruker D8, Bremen, Germany). A ESCALAB 250XI (Thermo Fisher Scientific, Waltham, MA, USA) photoelectron spectrophotometer was employed for XPS analyses. A JEM 2100 JEOL (Tokyo, Japan) electron microscope was employed for the TEM studies of the prepared samples. A Bruker VRTX70 (Bremen, Germany) model was used for FTIR analyses.

3.4. Photocatalytic Activity of Co_3O_4 -rGO

The photocatalytic performance of synthesized Co_3O_4 -rGO was assessed via the decomposition of methylene blue and methyl orange dyes. A UV–visible photometer was used to estimate the extent of the decomposition of selected dyes. To acquire the adsorption/desorption equilibrium in the photocatalytic experiment, a 50 mL solution of dye was stirred in the dark at a speed of 400 revolutions per minute after adding 0.1 g of Co_3O_4 -rGO. A sample of the reaction mixture was taken and analyzed. The reaction mixture was then stirred under solar irradiation. A total of 0.5 mL of the sample was removed from the mixture after a regular interval of 15 min and examined. For further analysis and to confirm the degradation of dye, COD and BOD measurements were employed. COD and BOD measurements were carried out on two samples, namely an untreated dye solution and a dye solution treated with Co_3O_4 -rGO, for 60 min.

For COD measurement, a 10 mL sample was taken in a reflux flask, and 1 mL of mercury sulphate solution (0.1 g HgSO_4 in 5 mL of concentrated sulfuric acid) was added to it. Then, 5 mL of potassium dichromate solution (6.13 g/L) was added, followed by the addition of 15 mL of silver sulfate–sulfuric acid solution (10 g/L sulfuric acid). The content was digested by refluxing for 2 h. After cooling to room temperature, a few drops of ferroin indicator were added to the mixture, which was titrated against the ferrous ammonium sulfate solution (9.8 g/20 mL sulfuric acid and 100 mL distilled water). The same procedure was repeated for the blank experiment, using distilled water instead of the sample. COD was calculated using the following equation:

$$\text{COD} = \frac{8 \times 1000 \times M(V_b - V_s)}{V_{\text{Sample}} \text{ (mL)}} \quad (7)$$

M: Molarity of ferrous ammonium sulfate solution;

V_b : Volume of ferrous ammonium sulfate solution consumed in the blank experiment;

V_b : Volume of ferrous ammonium sulfate solution consumed in the blank experiment;

V_s : Volume of ferrous ammonium sulfate solution consumed in a sample experiment.

The BOD was estimated by measuring dissolved oxygen. Specialized BOD bottles were filled with samples. The dissolved oxygen concentration was measured using a DO meter. The BOD bottles were incubated at 20 °C in the dark for 5 days. After incubation for 5 days, the dissolved oxygen concentration was measured again using a DO meter. The BOD was calculated by dividing the difference between the initial and final dissolved oxygen concentrations.

The BOD was estimated by measuring dissolved oxygen. Specialized BOD bottles were filled with samples. The dissolved oxygen concentration was measured using a DO meter. The BOD bottles were incubated at 20 °C in the dark for 5 days. After incubation for 5 days, the dissolved oxygen concentration was measured again using a DO meter. The BOD was calculated by the difference between the initial and final dissolved oxygen concentration.

4. Conclusions

The results and observations reported in this study indicate the importance and significance of the photocatalyst developed for the degradation of dyes. The general conclusions are extracted as follows:

1. The successful synthesis of Co_3O_4 -rGO was confirmed through characterization with XRD, XPS, TEM, and FTIR analyses.
2. The fabricated Co_3O_4 -rGO composite showed efficient catalytic performance in the photodegradation of MB and MO. The photocatalytic activity of Co_3O_4 -rGO was higher than the two-fold and three-fold catalytic activity of Co_3O_4 and rGO, respectively. The increase in the initial concentration of MB and MO resulted in a decrease in the photocatalytic performance.
3. About 98, 62, and 45% photodegradation of methylene blue was observed in 60 min of reaction using Co_3O_4 -rGO, Co_3O_4 , and rGO as photocatalysts, respectively. Similarly, the photodegradation of methyl orange was 92, 57, and 42% over Co_3O_4 -rGO, Co_3O_4 , and rGO as photocatalysts, respectively.
4. About 80% and 68% reductions in COD and BOD were detected in the 50 mL (200 mg/L) solution of MB/MO after treatment with Co_3O_4 -rGO for 60 min. The decrease in COD and BOD of the dye solutions indicates that Co_3O_4 -rGO can be employed as an efficient catalyst for the photodegradation of the dyes.
5. The enhanced photocatalytic efficiency of Co_3O_4 -rGO was attributed to the behavior of rGO as an electron reservoir that captures the photoexcited electron from Co_3O_4 .
6. The Co_3O_4 -rGO was found to be an efficient and reusable photocatalyst for the degradation of methylene blue and methyl orange.

Author Contributions: M.S.: conceptualization, methodology, writing—original draft preparation, supervision, visualization, project administration; A.N.: methodology, writing—original draft preparation, investigation; A.F.Z.: resources, writing—review and editing, data curation; F.H.A.: writing—original draft preparation, writing—review and editing, validation; A.I.: funding acquisition, writing—review and editing, data curation, formal analysis; A.A.A.-M.: writing—review and editing, formal analysis, validation; S.A.A.-H.: funding acquisition, writing—review and editing, investigation; M.E.A.Z.: funding acquisition, writing—review and editing, formal analysis, validation, project administration. All authors have read and agreed to the published version of the manuscript.

Funding: This work was supported and funded by the Deanship of Scientific Research at Imam Mohammad Ibn Saud Islamic University (IMSIU) (grant number IMSIU-RG23013).

Data Availability Statement: The data presented in this study are available.

Conflicts of Interest: The authors declare no conflict of interest.

References

1. Kamran, U.; Bhatti, H.N.; Noreen, S.; Tahir, M.A.; Park, S.J. Chemically Modified Sugarcane Bagasse-Based Biocomposites for Efficient Removal of Acid Red 1 Dye: Kinetics, Isotherms, Thermodynamics, and Desorption Studies. *Chemosphere* **2022**, *291*, 132796. [[CrossRef](#)]
2. Zafar, L.; Khan, A.; Kamran, U.; Park, S.J.; Bhatti, H.N. *Eucalyptus (camaldulensis)* Bark-Based Composites for Efficient Basic Blue 41 Dye Biosorption from Aqueous Stream: Kinetics, Isothermal, and Thermodynamic Studies. *Surf. Interfaces* **2022**, *31*, 101897. [[CrossRef](#)]
3. Yu, H.; Zhu, J.; Qiao, R.; Zhao, N.; Zhao, M.; Kong, L. Facile Preparation and Controllable Absorption of a Composite Based on PMo12/Ag Nanoparticles: Photodegradation Activity and Mechanism. *ChemistrySelect* **2022**, *7*, e202103668. [[CrossRef](#)]

4. Pang, S.; Zhou, C.; Sun, Y.; Zhang, K.; Ye, W.; Zhao, X.; Cai, L.; Hui, B. Natural Wood-Derived Charcoal Embedded with Bimetallic Iron/Cobalt Sites to Promote Ciprofloxacin Degradation. *J. Clean. Prod.* **2023**, *414*, 137569. [[CrossRef](#)]
5. Zheng, Y.; Liu, Y.; Guo, X.; Chen, Z.; Zhang, W.; Wang, Y.; Tang, X.; Zhang, Y.; Zhao, Y. Sulfur-Doped g-C₃N₄/RGO Porous Nanosheets for Highly Efficient Photocatalytic Degradation of Refractory Contaminants. *J. Mater. Sci. Technol.* **2020**, *41*, 117–126. [[CrossRef](#)]
6. Kim, S.; Kim, K.H.; Oh, C.; Zhang, K.; Park, J.H. Artificial Photosynthesis for High-Value-Added Chemicals: Old Material, New Opportunity. *Carbon Energy* **2022**, *4*, 21–44. [[CrossRef](#)]
7. Bankole, O.M.; Olaseni, S.E.; Adeyemo, M.A.; Ogunlaja, A.S. Microwave-Assisted Synthesis of Cobalt Oxide/Reduced Graphene Oxide (Co₃O₄-RGO) Composite and Its Sulfite Enhanced Photocatalytic Degradation of Organic Dyes. *Z. Fur. Phys. Chem.* **2020**, *234*, 1681–1708. [[CrossRef](#)]
8. Shah, K.W.; Li, W. A Review on Catalytic Nanomaterials for Volatile Organic Compounds VOC Removal and Their Applications for Healthy Buildings. *Nanomaterials* **2019**, *9*, 910. [[CrossRef](#)]
9. Xu, C.; Ravi Anusuyadevi, P.; Aymonier, C.; Luque, R.; Marre, S. Nanostructured Materials for Photocatalysis. *Chem. Soc. Rev.* **2019**, *48*, 3868–3902. [[CrossRef](#)]
10. Shi, H.; Zhang, F.; Shi, Q.; Li, M.; Dai, Y.; Zhang, Z.; Zhu, C. Responses of Arid Plant Species Diversity and Composition to Environmental Factors. *J. For. Res. (Harbin)* **2023**, *34*, 1723–1734. [[CrossRef](#)]
11. Poudel, M.B.; Awasthi, G.P.; Kim, H.J. Novel Insight into the Adsorption of Cr(VI) and Pb(II) Ions by MOF Derived Co-Al Layered Double Hydroxide @hematite Nanorods on 3D Porous Carbon Nanofiber Network. *Chem. Eng. J.* **2021**, *417*, 129312. [[CrossRef](#)]
12. Wang, Z.; Mei, Y.; Ling, J.; Yang, M.; Li, Y. Phthalimide Based New Photocatalysts Featured with Highly Selective Photodegradation of Azo-Dyes and Good Photocatalytic Activity in Both Homogeneous and Heterogeneous Systems. *J. Photochem. Photobiol. A Chem.* **2023**, *435*, 114346. [[CrossRef](#)]
13. Kumar, A.; Raorane, C.J.; Syed, A.; Bahkali, A.H.; Elgorban, A.M.; Raj, V.; Kim, S.C. Synthesis of TiO₂, TiO₂/PAni, TiO₂/PAni/GO Nanocomposites and Photodegradation of Anionic Dyes Rose Bengal and Thymol Blue in Visible Light. *Environ. Res.* **2023**, *216*, 114741. [[CrossRef](#)] [[PubMed](#)]
14. Khan, I.; Luo, M.; Khan, S.; Asghar, H.; Saeed, M.; Khan, S.; Khan, A.; Humayun, M.; Guo, L.; Shi, B. Green synthesis of SrO bridged LaFeO₃/g-C₃N₄ nanocomposites for CO₂ conversion and bisphenol A degradation with new insights into mechanism. *Environ. Res.* **2022**, *207*, 112650. [[CrossRef](#)] [[PubMed](#)]
15. Kotp, Y.H. Fabrication of Cerium Titanate Cellulose Fiber Nanocomposite Materials for the Removal of Methyl Orange and Methylene Blue from Polluted Water by Photocatalytic Degradation. *Environ. Sci. Pollut. Res.* **2022**, *29*, 81583–81608. [[CrossRef](#)]
16. Eissa, D.; Hegab, R.H.; Abou-Shady, A.; Kotp, Y.H. Green Synthesis of ZnO, MgO and SiO₂ Nanoparticles and Its Effect on Irrigation Water, Soil Properties, and Origanum Majorana Productivity. *Sci. Rep.* **2022**, *12*, 5780. [[CrossRef](#)]
17. Deng, J.; Lei, W.; Fu, J.; Jin, H.; Xu, Q.; Wang, S. Enhanced Selective Photooxidation of Toluene to Benzaldehyde over Co₃O₄-Modified BiOBr/AgBr S-Scheme Heterojunction. *Sol. RRL* **2022**, *6*, 2200279. [[CrossRef](#)]
18. Xu, Q.; Xia, Z.; Zhang, J.; Wei, Z.; Guo, Q.; Jin, H.; Tang, H.; Li, S.; Pan, X.; Su, Z.; et al. Recent Advances in Solar-Driven CO₂ Reduction over g-C₃N₄-Based Photocatalysts. *Carbon Energy* **2023**, *5*, e205.
19. Mousavi, M.; Habibi-Yangjeh, A.; Pouran, S.R. Review on Magnetically Separable Graphitic Carbon Nitride-Based Nanocomposites as Promising Visible-Light-Driven Photocatalysts. *J. Mater. Sci. Mater. Electron.* **2018**, *29*, 1719–1747. [[CrossRef](#)]
20. Rao, G.; Zhao, H.; Chen, J.; Deng, W.; Jung, B.; Abdel-Wahab, A.; Batchelor, B.; Li, Y. FeOOH and Fe₂O₃ Co-Grafted TiO₂ Photocatalysts for Bisphenol A Degradation in Water. *Catal. Commun.* **2017**, *97*, 125–129. [[CrossRef](#)]
21. Moussa, H.; Chouchene, B.; Gries, T.; Balan, L.; Mozet, K.; Medjahdi, G.; Schneider, R. Growth of ZnO Nanorods on Graphitic Carbon Nitride GCN Sheets for the Preparation of Photocatalysts with High Visible-Light Activity. *ChemCatChem* **2018**, *10*, 4987–4997. [[CrossRef](#)]
22. Saeed, M.; Usman, M.; Ibrahim, M.; ul Haq, A.; Khan, I.; Ijaz, H.; Akram, F. Enhanced Photo Catalytic Degradation of Methyl Orange Using p-n Co₃O₄-TiO₂ Hetero-Junction as Catalyst. *Int. J. Chem. React. Eng.* **2020**, *18*, 20200004. [[CrossRef](#)]
23. Saeed, M.; Muneer, M.; Khosa, M.K.K.; Akram, N.; Khalid, S.; Adeel, M.; Nisar, A.; Sherazi, S. *Azadirachta indica* Leaves Extract Assisted Green Synthesis of Ag-TiO₂ for Degradation of Methylene Blue and Rhodamine B Dyes in Aqueous Medium. *Green Process. Synth.* **2019**, *8*, 659–666. [[CrossRef](#)]
24. Tan, X.Q.; Ng, S.F.; Mohamed, A.R.; Ong, W.J. Point-to-Face Contact Heterojunctions: Interfacial Design of 0D Nanomaterials on 2D g-C₃N₄ towards Photocatalytic Energy Applications. *Carbon Energy* **2022**, *4*, 665–730. [[CrossRef](#)]
25. Poudel, M.B.; Yu, C.; Kim, H.J. Synthesis of Conducting Bifunctional Polyaniline@mn-TiO₂ Nanocomposites for Supercapacitor Electrode and Visible Light Driven Photocatalysis. *Catalysts* **2020**, *10*, 546. [[CrossRef](#)]
26. Peng, W.; Li, H.; Liu, Y.; Song, S. A Review on Heavy Metal Ions Adsorption from Water by Graphene Oxide and Its Composites. *J. Mol. Liq.* **2017**, *230*, 496–504. [[CrossRef](#)]
27. Hernández-Gordillo, A.; Obregón, S.; Paraguay-Delgado, F.; Rodríguez-González, V. Effective Photoreduction of a Nitroaromatic Environmental Endocrine Disruptor by AgNPs Functionalized on Nanocrystalline TiO₂. *RSC Adv.* **2015**, *5*, 15194–15197. [[CrossRef](#)]
28. Wang, L.; Du, Y.; Zhu, Q.; Song, J.; Ou, K.; Xie, G.; Yu, Z. Regulating the Alkyl Chain Length of Quaternary Ammonium Salt to Enhance the Inkjet Printing Performance on Cationic Cotton Fabric with Reactive Dye Ink. *ACS Appl. Mater. Interfaces* **2023**, *15*, 19750–19760. [[CrossRef](#)]

29. Zhang, J.; Zhong, A.; Huang, G.; Yang, M.; Li, D.; Teng, M.; Han, D. Enhanced Efficiency with CDCA Co-Adsorption for Dye-Sensitized Solar Cells Based on Metallosalophen Complexes. *Sol. Energy* **2020**, *209*, 316–324. [[CrossRef](#)]
30. Munde, A.V.; Mulik, B.B.; Dighole, R.P.; Sathe, B.R. Cobalt Oxide Nanoparticle-Decorated Reduced Graphene Oxide (Co₃O₄-RGO): Active and Sustainable Nanoelectrodes for Water Oxidation Reaction. *New J. Chem.* **2020**, *44*, 15776–15784. [[CrossRef](#)]
31. Garakani, M.A.; Abouali, S.; Zhang, B.; Takagi, C.A.; Xu, Z.L.; Huang, J.Q.; Huang, J.; Kim, J.K. Cobalt Carbonate/ and Cobalt Oxide/Graphene Aerogel Composite Anodes for High Performance Li-Ion Batteries. *ACS Appl. Mater. Interfaces* **2014**, *6*, 18971–18980. [[CrossRef](#)]
32. Zhang, Y.; Liu, G. Development of Highly Efficient and Durable Reduced Graphene Oxide Decorated with Ag/Co₃O₄ Nanocomposite towards Photocatalytic C[Sbnd]H Activation. *J. Photochem. Photobiol. A Chem.* **2020**, *394*, 112494. [[CrossRef](#)]
33. Shahid, M.M.; Rameshkumar, P.; Numan, A.; Shahabuddin, S.; Alizadeh, M.; Khiew, P.S.; Chiu, W.S. A Cobalt Oxide Nanocubes Interleaved Reduced Graphene Oxide Nanocomposite Modified Glassy Carbon Electrode for Amperometric Detection of Serotonin. *Mater. Sci. Eng. C* **2019**, *100*, 388–395. [[CrossRef](#)]
34. Li, D.; Shi, D.; Chen, Z.; Liu, H.; Jia, D.; Guo, Z. Enhanced Rate Performance of Cobalt Oxide/Nitrogen Doped Graphene Composite for Lithium Ion Batteries. *RSC Adv.* **2013**, *3*, 5003–5008. [[CrossRef](#)]
35. Nguyen, D.C.T.; Cho, K.Y.; Oh, W.C. Synthesis of Frost-like CuO Combined Graphene-TiO₂ by Self-Assembly Method and Its High Photocatalytic Performance. *Appl. Surf. Sci.* **2017**, *412*, 252–261. [[CrossRef](#)]
36. Tran, M.H.; Jeong, H.K. Synthesis and Characterization of Silver Nanoparticles Doped Reduced Graphene Oxide. *Chem. Phys. Lett.* **2015**, *630*, 80–85. [[CrossRef](#)]
37. Verma, S.; Mungse, H.P.; Kumar, N.; Choudhary, S.; Jain, S.L.; Sain, B.; Khatri, O.P. Graphene Oxide: An Efficient and Reusable Carbocatalyst for Aza-Michael Addition of Amines to Activated Alkenes. *Chem. Commun.* **2011**, *47*, 12673–12675. [[CrossRef](#)]
38. Hu, C.; Lu, T.; Chen, F.; Zhang, R. A Brief Review of Graphene–Metal Oxide Composites Synthesis and Applications in Photocatalysis. *J. Chin. Adv. Mater. Soc.* **2013**, *1*, 21–39. [[CrossRef](#)]
39. Al Nafiey, A.; Addad, A.; Sieber, B.; Chastanet, G.; Barras, A.; Szunerits, S.; Boukherroub, R. Reduced Graphene Oxide Decorated with Co₃O₄ Nanoparticles (RGO-Co₃O₄) Nanocomposite: A Reusable Catalyst for Highly Efficient Reduction of 4-Nitrophenol, and Cr(VI) and Dye Removal from Aqueous Solutions. *Chem. Eng. J.* **2017**, *322*, 375–384. [[CrossRef](#)]
40. Jha, A.; Mhamane, D.; Suryawanshi, A.; Joshi, S.M.; Shaikh, P.; Biradar, N.; Ogale, S.; Rode, C.V. Triple Nanocomposites of CoMn₂O₄, Co₃O₄ and Reduced Graphene Oxide for Oxidation of Aromatic Alcohols. *Catal. Sci. Technol.* **2014**, *4*, 1771–1778. [[CrossRef](#)]
41. Taourati, R.; Khaddor, M.; el Kasmi, A. Stable ZnO Nanocatalysts with High Photocatalytic Activity for Textile Dye Treatment. *Nano-Struct. Nano-Objects* **2019**, *18*, 100303. [[CrossRef](#)]
42. Kumbhakar, P.; Pramanik, A.; Biswas, S.; Kole, A.K.; Sarkar, R.; Kumbhakar, P. In-Situ Synthesis of RGO-ZnO Nanocomposite for Demonstration of Sunlight Driven Enhanced Photocatalytic and Self-Cleaning of Organic Dyes and Tea Stains of Cotton Fabrics. *J. Hazard. Mater.* **2018**, *360*, 193–203. [[CrossRef](#)] [[PubMed](#)]
43. Raizada, P.; Sudhaik, A.; Patial, S.; Hasija, V.; Parwaz Khan, A.A.; Singh, P.; Gautam, S.; Kaur, M.; Nguyen, V.H. Engineering Nanostructures of CuO-Based Photocatalysts for Water Treatment: Current Progress and Future Challenges. *Arab. J. Chem.* **2020**, *13*, 8424–8457. [[CrossRef](#)]
44. Wang, M.; Wang, J.; Xi, C.; Cheng, C.; Zou, C.; Zhang, R.; Xie, Y.; Guo, Z.; Tang, C.; Dong, C.; et al. A Hydrogen-Deficient Nickel–Cobalt Double Hydroxide for Photocatalytic Overall Water Splitting. *Angew. Chem.* **2020**, *132*, 11607–11612. [[CrossRef](#)]
45. Ahmad, M.; Ahmed, E.; Hong, Z.L.; Xu, J.F.; Khalid, N.R.; Elhissi, A.; Ahmed, W. A Facile One-Step Approach to Synthesizing ZnO/Graphene Composites for Enhanced Degradation of Methylene Blue under Visible Light. *Appl. Surf. Sci.* **2013**, *274*, 273–281. [[CrossRef](#)]
46. Song, C.; Wang, L.J.; Sun, S.M.; Wu, Y.; Xu, L.J.; Gan, L. Preparation of Visible-Light Photocatalysts of Bi₂O₃/Bi Embedded in Porous Carbon from Bi-Based Metal Organic Frameworks for Highly Efficient Rhodamine B Removal from Water. *Xinxing Tan Cailiao/New Carbon Mater.* **2020**, *35*, 609–618. [[CrossRef](#)]
47. Saeed, M.; Alwadai, N.; ben Farhat, L.; Baig, A.; Nabgan, W.; Iqbal, M. Co₃O₄-Bi₂O₃ Heterojunction: An Effective Photocatalyst for Photodegradation of Rhodamine B Dye. *Arab. J. Chem.* **2022**, *15*, 103732. [[CrossRef](#)]
48. Zada, N.; Saeed, K.; Khan, I. Decolorization of Rhodamine B Dye by Using Multiwalled Carbon Nanotubes/Co–Ti Oxides Nanocomposite and Co–Ti Oxides as Photocatalysts. *Appl. Water Sci.* **2020**, *10*, 40. [[CrossRef](#)]
49. Saroyan, H.; Kyzas, G.Z.; Deliyanni, E.A. Effective Dye Degradation by Graphene Oxide Supported Manganese Oxide. *Process.* **2019**, *7*, 40. [[CrossRef](#)]
50. Saeed, M.; Albalawi, K.; Khan, I.; Akram, N.; Abd El-Rahim, I.H.A.; Alhag, S.K.; Ezzat Ahmed, A. Faiza Synthesis of P-n NiO-ZnO Heterojunction for Photodegradation of Crystal Violet Dye. *Alex. Eng. J.* **2022**, *65*, 561–574. [[CrossRef](#)]
51. Jiao, T.; Guo, H.; Zhang, Q.; Peng, Q.; Tang, Y.; Yan, X.; Li, B. Reduced Graphene Oxide-Based Silver Nanoparticle-Containing Composite Hydrogel as Highly Efficient Dye Catalysts for Wastewater Treatment. *Sci. Rep.* **2015**, *5*, 11873. [[CrossRef](#)] [[PubMed](#)]
52. Liu, W.; Cai, J.; Li, Z. Self-Assembly of Semiconductor Nanoparticles/Reduced Graphene Oxide (RGO) Composite Aerogels for Enhanced Photocatalytic Performance and Facile Recycling in Aqueous Photocatalysis. *ACS Sustain. Chem. Eng.* **2015**, *3*, 277–282. [[CrossRef](#)]
53. Ding, Y.; Zhou, Y.; Nie, W.; Chen, P. MoS₂–GO Nanocomposites Synthesized via a Hydrothermal Hydrogel Method for Solar Light Photocatalytic Degradation of Methylene Blue. *Appl. Surf. Sci.* **2015**, *357*, 1606–1612. [[CrossRef](#)]

54. Choi, J.; Reddy, D.A.; Islam, M.J.; Ma, R.; Kim, T.K. Self-Assembly of CeO₂ Nanostructures/Reduced Graphene Oxide Composite Aerogels for Efficient Photocatalytic Degradation of Organic Pollutants in Water. *J. Alloys Compd.* **2016**, *688*, 527–536. [[CrossRef](#)]
55. Cai, R.; Wu, J.G.; Sun, L.; Liu, Y.J.; Fang, T.; Zhu, S.; Li, S.Y.; Wang, Y.; Guo, L.F.; Zhao, C.E.; et al. 3D Graphene/ZnO Composite with Enhanced Photocatalytic Activity. *Mater. Des.* **2016**, *90*, 839–844. [[CrossRef](#)]
56. Cai, J.; Liu, W.; Li, Z. One-Pot Self-Assembly of Cu₂O/RGO Composite Aerogel for Aqueous Photocatalysis. *Appl. Surf. Sci.* **2015**, *358*, 146–151. [[CrossRef](#)]
57. Qiu, B.; Xing, M.; Zhang, J. Mesoporous TiO₂ Nanocrystals Grown in Situ on Graphene Aerogels for High Photocatalysis and Lithium-Ion Batteries. *J. Am. Chem. Soc.* **2014**, *136*, 5852–5855. [[CrossRef](#)]
58. Qiu, B.; Deng, Y.; Du, M.; Xing, M.; Zhang, J. Ultradispersed Cobalt Ferrite Nanoparticles Assembled in Graphene Aerogel for Continuous Photo-Fenton Reaction and Enhanced Lithium Storage Performance. *Sci. Rep.* **2016**, *6*, 29099. [[CrossRef](#)]
59. Luo, J.; Zhang, N.; Lai, J.; Liu, R.; Liu, X. Tannic Acid Functionalized Graphene Hydrogel for Entrapping Gold Nanoparticles with High Catalytic Performance toward Dye Reduction. *J. Hazard. Mater.* **2015**, *300*, 615–623. [[CrossRef](#)]

Disclaimer/Publisher’s Note: The statements, opinions and data contained in all publications are solely those of the individual author(s) and contributor(s) and not of MDPI and/or the editor(s). MDPI and/or the editor(s) disclaim responsibility for any injury to people or property resulting from any ideas, methods, instructions or products referred to in the content.